Materials Science & Engineering A 875 (2023) 145075

Contents lists available at ScienceDirect

Materials Science & Engineering A

journal homepage: www.elsevier.com/locate/msea

Use of miniaturized tensile specimens to evaluate the ductility and formability of dual phased steels for Rapid Alloy Prototyping

Lintao Zhang *, Will Harrison, Mazher A. Yar, Shahin Mehraban, Stephen G.R. Brown, Nicholas P. Lavery

Future Manufacturing Research Institute, College of Engineering, Swansea University, Bay Campus, Fabian Way, Swansea SA1 8EN, UK

ARTICLE INFO

Keywords:
Dual-phase steel
Size effect
Total elongation
Materials constant
Rapid alloy prototyping (RAP)

ABSTRACT

This work aims to investigate feasibility of using non-standard miniaturized tensile specimens (MTS) to characterize total elongation and formability behaviour of dual phase steels: to establish the scaling rules for MTS to predict a range of mechanical properties of steels obtained through rapid alloy prototyping (RAP) in the laboratory. Accurate measurement of these properties using miniature specimens allows the formability behaviour of materials produced using RAP, a process which can produce lab scale samples of < 100 grams. This allows the effects of multiple compositions and thermomechanical processing parameters on formability to be evaluated. For this study, the ability of miniature tensile specimens to characterize ductility, forming limits and r-values has been compared to properties measured using standard sized tensile specimens for the dual phase steels, DP600 and DP800. 5 different tensile specimens were investigated, with gauge lengths varying from 80 mm to 5 mm and samples were taken at different orientations to the rolling direction. Total elongation was evaluated against slimness ratio for each tensile sample using the Bertelle–Oliver method and good correlations were obtained, despite specimen thicknesses being below the critical value, and the tensile strength of DP800 exceeding the limit stated for the method. Forming limit curves (FLC) were predicted using the Keeler–Brazier method, based on tensile data obtained using the standard and non-standard tensile specimens These curves compared favourably to experimentally obtained FLCs, however the curve predicted using the miniaturized tensile specimen over-predicted the major strain. The anisotropy of the rolled sheet steels was characterized from r-values obtained from tensile tests performed at different orientations to the rolling direction. Values obtained from the miniature tensile test were comparable to those obtained from standard tests within the range of scatter. The results obtained through this study provide confidence in using the miniature tensile specimens to predict the formability of heterogeneous alloys such as DP steels, manufactured using the RAP process.

1. Introduction

Dual-phase (DP) steel refers to a category of high-strength low-alloy (HSLA) steel with two phases: a ferrite matrix and a dispersed second phase of martensite [1] and it was first patented in USA in 1968 [2]. The development of DP steel was started in the 1970s, driven by the demand of automotive industry: approximately 74% of the steels used in the automotive industry are DP grade at present [3]. DP steels have contributed to the structural integrity of automotive structures due to its high strength in thin sections. This allows crash-worthiness to be maintained whilst reducing the weight of components, thus improving performance and reducing fuel use. The mechanical properties of these steels are strongly dependent both chemical composition and thermo-mechanical processing. The wide application of DP steels has led to much interest into the effects of residual elements and processing on the final product properties as well as how to develop new similar steel grades more efficiently.

To manufacture new steels, or variations of existing steel, the traditional route is to use vacuum induction melt (VIM) cast with a scale of 25 to 60 kg. Rapid alloy prototyping (RAP) is a new process to develop steels using small amount of materials, 20 to 140 g, at the lab scale [4], with a target of 100 compositions being made and tested per week. Compared to VIM, RAP accelerates the process and gives more flexibility, which are critical to the laboratory scale development. Zhu et al. proved that the replication of the industrial DP800 product within the lab can significantly reduce the turn-around time for product development: 72 tensiles or 20 hole expansion tests could be completed

* Corresponding author.
E-mail address: L.Zhang@Swansea.ac.uk (L. Zhang).

https://doi.org/10.1016/j.msea.2023.145075
Received 16 December 2022; Received in revised form 6 April 2023; Accepted 21 April 2023
Available online 24 April 2023

Table 1
Chemical composition of DP800 and DP600 (% weight).

	C	Si	Mn	P	S	Ni	Cu	Cr	Fe
DP800	0.136	0.249	1.77	0.011	0.0027	0.018	0.024	0.558	Balance
DP600	0.098	0.244	1.705	0.015	0.004	0.023	0.018	0.548	Balance

within around two weeks [5]. A combination of rapid alloy prototyping techniques, such as high-throughput experimentation, combinatorial synthesis, and additive manufacturing can also be used to develop and evaluate new DP grades effectively. Wen et al. manufactured intensive dual-phase steels through laser additive manufacturing method and the expected stress value has been achieved for the materials made [6]: the tensile strengths along the scanning direction and the transversal direction were in the range of 850 to 1000 MPa.

However, small amount of materials raises a question: the standard tensile specimen, e.g. ISO/EN A80, is too large to be extracted from a strip manufactured through the RAP process [7]. Instead, a non-standard miniaturized tensile specimen (MTS) must be used. This requires to design a non-standard MTS, which could be used not only for the dual phase steel but also for unknown materials manufactured by the RAP process in future. The comparisons of yield strength, tensile strength and the uniform elongation between standard specimens and non-standard MTS were previously studied [7]. However, the effects of using a sub-sized tensile specimens on total elongation measurements for these steels is not documented.

Bertella–Oliver equation has been wildly used to compare the elongation measurements between different test piece dimensions [8]:

$$e_f = e_0 K^{-\alpha}, \tag{1}$$

where e_f, e_0, K and α denote the total elongation, specific elongation (the percentage elongation for unit gauge length and the unit cross sectional area), the slimness ratio (gauge length over the square root of cross-section area) of the test piece and the material constant, respectively. A number of investigations have focused on determining the values of e_0 and α in Eq. (1) for different materials under different conditions. Yang et al. investigated miniatured tensile specimens by varying the bar's gauge length (3 to 25 mm) and thickness (0.2 to 3 mm) to determine the size effect on e_f for A588 steel [9]. This study found that the specific elongation e_0 and the material constant α are 66 and −0.6 in the K range 0.5 to 6. Xu et al. studied the validity of Oliver's rule for high strength pipeline steel X65, X70, X80 and X90 and the material constant values α were determined [10]. Takeda et al. studied the relationship between the total elongation and the tensile specimen thickness (0.2, 0.5, 1.2 and 2.0 mm) with a fixed gauge length (20 mm) for industrially pure iron [11]. The results indicated that a poor correlation between K and e_f was found for the given range of K values. This is due to the increase in stress triaxiality as specimen thickness decreased. Hanlon et al. studied the size effect of 22MnB5 alloy [12] for a range of standard tensile specimens. The standard specimens used were: ISO/EN A80, ISO/EN A50, JIS5, ASTM50 and ASTM25, with thicknesses ranging from 1 to 4 mm. Different values of the material constant α (0.4, 0.65 and 0.9 respectively) were used to fit the total elongation data. A spherodized 4130 steel (tensile strength > 1500 MPa, thickness 3.2 to 12.95 mm, gauge length 25 and 50 mm) was adopted to study the relationship between the total elongation and cross-sectional area/thickness [13]. In both these cases, there was a relatively poor fit to the elongation data and this may have been because for these alloys, the strength was above the 700 MPa: the upper limit for the Bertella–Oliver method [14].

This study focuses on whether MTS can be used to predict e_f values, comparable to those obtained from full size standard tensile specimens. The study will also investigate the effects of specimen size on the hardening exponent obtained for DP steels. This will help to understand how reliable MTS can be in evaluating the ductility and formability of steels made using the RAP process. To answer the following question are the main tasks and novelties of this work:

1. Is the Bertella–Oliver equation valid for dual phase steels, especially for the strip with a thinner thickness (>2 mm) and a higher tensile strength (>700 MPa), is compared to the standard [14]?
2. What are the specific elongation values and material constants for DP600 and DP800 steels, if the Bertella–Oliver equation is valid for them? These have never been reported before, according to the authors knowledge. Will the alignment of the specimen with respect to the rolling direction be important and how does it affect these constants?
3. How accurate are the non-standard MTS in measuring elongation and formability properties of the material obtained from RAP routine?

The outline of paper is as follows. The materials and methods are introduced in Section 2. Section 3.1 and Section 3.2 aim at determining specific elongation and material constant for DP600 and DP800, respectively. These constants were compared in Section 3.3. These three sections will answer the question 1 and 2, which are raised above. In Section 3.4, the performance of designed non-standard miniaturized tensile specimens, proposed to be used for RAP, on predicting total elongation e_f, forming limit curves and plastic strain ratio in Section 3.4.1, Section 3.4.2 and Section 3.4.3, respectively. This section will answer the question 3. Main conclusions are summarized in Section 4

2. Materials and methods

2.1. Materials

DP600 and DP800 steels were used for this study as they are widely used. Table 1 and Fig. 1 show their chemical composition and engineering stress strain curves, respectively. It is to be noted that DP800 could be more challenging in terms of the specimen size effect on e_f due to its ultimate tensile strength being above the Standard's upper bound of 700 MPa to apply Bertelle–Oliver equation [14]. The microstructure of both DP grades have a relatively soft Ferrite matrix, with a dispersion of much harder Martensite islands. The volume fractions of each phase were determined using multiple scanning electron microscope (SEM)images, such as those shown in Fig. 1. The image analysis software, ImageJ, was used to measure Ferrite volume fractions of 70% and 77% for DP800 and DP600.

2.2. Geometries

Tensile specimens with five different dimensions were designed and manufactured. The dimensions of these specimens include three standard bars: ISO/EN A80, ISO/EN A50 and ASTM25 and two non-standard MTS namely: Mini1 and Mini2, respectively. Table 2 shows the detailed dimensions of the tensile specimens. Fig. 2 showed the definitions of the variables showed in Table 2. The samples were manufactured from commercially available DP800 and DP600 final product. Therefore, the thickness of the tensile bars are constant: 1.2 mm and 1.6 mm for DP800 and DP600, respectively. A80, A50, ASTM25 and Mini1 test pieces were made through computer numerical control (CNC) machining and Mini2 test pieces were manufactured by electrical discharge machining (EDM) methods to minimize deformation, prior to testing. The surface roughness of the bars is small enough to conduct tensile test without influencing the results [7]. The tensile bars were taken from similar region of the sheet to reduce potential variability associated with sample location. For all the specimens, the slimness ratios are less than 25 and the aspect ratios (width/thickness) are smaller than 20, which comply with the limit values to adopt Bertelle–Oliver equation according to the standard.

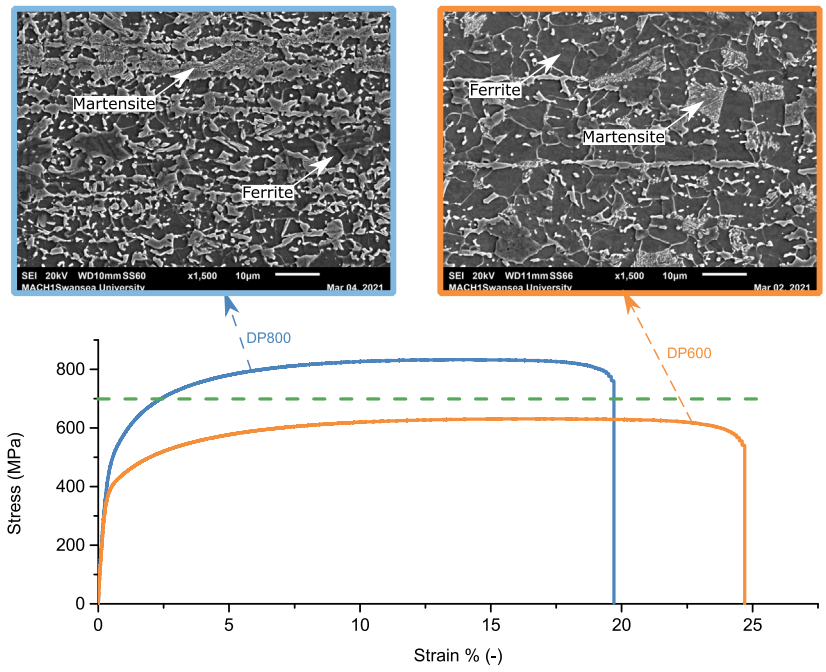

Fig. 1. Engineering stress strain curves and typical microstructure of the adopted dual-phase steels in this work: DP800 and DP600. DP800 has higher ultimate tensile strength due to its higher martensite phase ratio. The dashed line denotes the upper bound stress (700 MPa) to apply Bertelle–Oliver equation.

Table 2
Tested tensile bar dimensions. L_t, L_c, L_o, b_0, R and a_0 denote the total length of test piece, parallel length, gauge length, original width of the parallel length of a flat test piece, the shoulder radius and the thickness of the bar, respectively. No. denotes the number of the tests for each dimension and material.

		L_t (mm)	L_c (mm)	L_o (mm)	b_0 (mm)	R (–)	L_o/L_c (–)	L_o/b_0 (–)	$(L_c\text{-}2b_0)/L_0$ (–)	a_0 (mm)	K (–)	No. (–)
A80	DP800	260	120	80	20	25	0.67	4	1	1.2	16.33	2
	DP600									1.6	14.14	2
A50	DP800	200	75	50	12.5	15	0.67	4	1	1.2	12.91	6
	DP600									1.6	11.18	6
ASTM25	DP800	76	32	25	9	6	0.78	4.17	0.8	1.2	9.32	10
	DP600									1.6	8.07	6
Mini1	DP800	60	12.5	10	3	3	0.8	3.33	0.65	1.2	5.27	14
	DP600									1.6	4.56	6
Mini2	DP800	41	9	5	2	1.5	0.56	2.5	1	1.2	3.23	37
	DP600									1.6	2.80	12

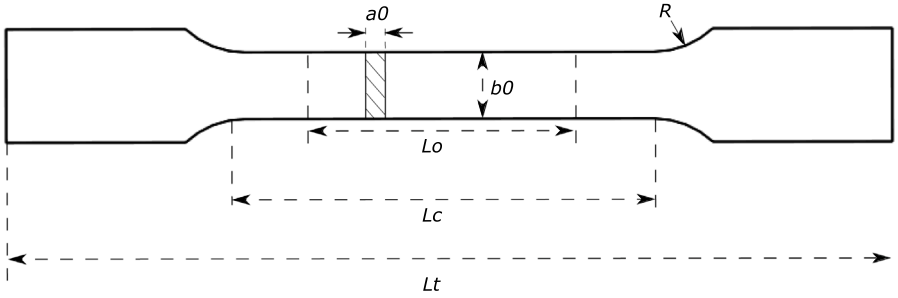

Fig. 2. Definition of L_t, L_c, L_o, a_0, b_0 and R showed in Table 2.

2.3. Methods

2.3.1. Tensile test and microstructure analysis

Tensile tests were conducted on a Tinius-Olsen H25KS uniaxial tensile machine. The machine has a 25 kN force capacity with an accuracy of ±0.5% of applied load from 2 to 100% of the load cell capacity and ±1% down to 1% of the load cell capacity. The strain was captured by a video extensometer (XSight 9MPX). A fixed cross-head velocity of 1 mm/min was used for all bars where a strain rate sensitivity test was reported in previous research [7]. Before testing, the outlines of the bars were checked by a profile projector Shadowgraph to ensure that the gauge sections were within specified tolerances. The averaged width and thickness values, measured at 3 locations in the gauge length section, were adopted for subsequent calculations. The microstructure analysis was conducted using a JEOL 6010 Scanning Electron Microscope using a 20 KV accelerating voltage and Secondary Electron Detector.

2.3.2. DP800 plastic strain ratio (r-value) measurement

Specimens with dimensions of A80, A50, ASTM25 and Mini1 were adopted to determine size effect on the DP800 r-values. Identical tensile machine, compared to that in Section 2.3.1, was used to conduct the experiment. Different strain rates were used: the strain rates for Range 2 and 4 are 2.5 $\times 10^{-4}$ 1/s and 6.7 $\times 10^{-3}$ 1/s, which according to standard [15]. Variable strain rate intends to minimize the variation of the test rates during the moment when strain rate sensitive parameters are determined and to minimize the measurement uncertainty of the test results. Range 2 and 4 are defined as the range in the plastic region: from the start till post yield strength (after lower yield strength) and the stage between lower yield strength and the fracture point. The r-values were calculated through the following equation:

$$r = \frac{-\epsilon_w}{\epsilon_w + \epsilon_l}, \tag{2}$$

where ϵ_w and ϵ_l denote the width and length strains.

2.3.3. Specific elongation and material constant determination

There are usually two methods to determine the values of e_0 and α in Eq. (1). Method I is to fit all the existing experimental data based on different specimens (different K values) [9,16] and thus to determine these constants. Method II involves replacing the specific elongation by using one of the existing results (e_f^{ref} and K^{ref}) as a reference, to find the value of material constant [11,12]:

$$\begin{aligned} e_f &= e_f^{ref} \cdot \left(\frac{\frac{L^{ref.}}{\sqrt{A}^{ref.}}}{\frac{L}{\sqrt{A}}}\right)^{\hat{\alpha}} \\ &= e_f^{ref} \cdot \left(\frac{K^{ref.}}{K}\right)^{\hat{\alpha}}. \end{aligned} \tag{3}$$

The specific elongation determined through Method II ($\hat{e_0}$) equals $e_f^{ref}/(K^{ref})^{\hat{\alpha}}$. The values of e_0, α (determined through Method I) and $\hat{e_0}$ $\hat{\alpha}$ (determined through Method II) may be different.

In this work, Method I and II were both used based on the tensile test results of five different dimensions. Method I is straightforward. The following steps were introduced for Method II (A80 as the reference geometry):

1. Calculate A80 specimen as K^{ref},
2. Calculate the averaged e_f based on A80 specimens' tests as $\bar{e_f}^{ref}$ (if multiple tests were conducted based on A80 bars),
3. Calculate other specimen's (A50, ASTM25, Mini1 and Mini2) K and $\bar{e_f}$ values (if multiple tests were conducted based on A50, ASTM25, Mini1 and Mini2 bars),
4. Determine $\hat{\alpha}^i$ and $\hat{e_0^i}$ between the other specimen and the reference dimension by using equation:

$$\hat{\alpha}^i = \frac{Ln(\bar{e_f}^i) - Ln(\bar{e_f}^{ref})}{Ln(K^i) - Ln(K^{ref})}, \tag{4}$$

$$\hat{e_0}^i = e_f^{ref}/(K^{ref})^{\hat{\alpha}}, \tag{5}$$

   where i denotes the other specimens dimensions, e.g. A50, ASTM25, Mini1 and Mini2,
5. To average $\hat{\alpha}^i$ (and $\hat{e_o}^i$) as the material constant (and specific elongation) $\hat{\alpha}$ (and $\hat{e_o}$) based on A80 in the K range from K^{mini2} to K^{A80}.
6. By using the determined $\hat{\alpha}$, K^{ref} and $\bar{e_f}^{ref}$ values, the predicted e_f can be obtained if K is given.

2.3.4. Strain hardening exponent and forming limit curve

In this work, Keeler–Brazier formula was used to determine the forming limit curves [17]:

$$\epsilon_1 = \begin{cases} FLD_0 + \epsilon_2(0.784854 - 0.008565 \times \epsilon_2) & \epsilon_2 \le 0, \\ FLD_0 + \epsilon_2(0.027254 \times \epsilon_2 - 1.1965) & \epsilon_2 > 0, \end{cases} \tag{6}$$

where FLD_0 is:

$$FLD_0 = \frac{n}{0.2116}(23.25 + 356.1 \times C_1), \tag{7}$$

where C_1 is:

$$C_1 = \begin{cases} t & t \le 0.0118, \\ 0.0118 & t > 0.0118, \end{cases} \tag{8}$$

where ϵ_1, ϵ_2, n and t stand for major strain, minor strain, strain hardening exponent and plate metal thickness, respectively. The thickness of DP800 sheet is 1.2 mm and n values were determined through Hollomon strain-hardening equation [18]:

$$\sigma = k\epsilon_p^n, \tag{9}$$

where k is strength coefficient, which is defined as the true strength at a true strain of 1.

3. Results and discussion

3.1. e_0 and α determination through Method I

Fig. 3 shows the log–log plots of the relationship between e_f and K for DP600 and DP800 steel for all tensile specimens $K \in (2.8\ 14.14)$ and $\in (3.23\ 16.33)$ for DP600 and DP800 respectively. K = 4.52 and 5.65 (dashed lines in Fig. 3 (a) and (c)) are the standard tensile specimens' K values based on the ASTM E8/E8M [19] and ISO-6892-1 [20], respectively.

Firstly, for both steels, based on the mean e_f value, good fits (minimum $R^2 > 0.97$) of e_f are achieved for specimens taken parallel to the rolling direction (RD) and traverse to the rolling direction (TD) to the rolling direction for both DP600, Fig. 3(a) and (b) and DP800, Fig. 3(c) and (d). Good fits indicate that the Bertelle–Oliver equation is valid for both DP600 and DP800 steel, despite the UTS of DP800 being higher than the rule's upper bound (~700 MPa) and the strip thickness is less than the minimum specified (2 mm). Therefore, the e_0 and α values were determined for DP600 and DP800 according to fitting expressions, as showed in the figure. Secondly, it is worth noting that for DP600, the specimen's orientation has little effect on e_0 and α values as these constants' divergences between RD-bar and TD-bar are 9.6% and 0.8%, respectively. However, the tensile bar's orientation plays a role for DP800 on these constants: the divergences of them between RD-bar and TD-bar are 21.1% and 71.1%, respectively. This is due to that the fact that for high strength steel is typically harder and less ductile than lower strength steels, and as a result, it can be more sensitive to variations in the orientation of the test specimen. The microstructure of high strength steel, DP800 for instance, is highly anisotropic, meaning that its properties are more sensitive to tensile bars orientation. Thirdly, the results indicated that the RD-bar is more ductile than the TD-bar, which is true for both DP600 and DP800. This is due to the presence of elongated martensite islands, the morphology of which are strongly influenced by processing. For tensile tests with the loading direction transverse to rolling direction (TD-bar), the principle stress acts across the elongated grains, resulting in a larger number of ferrite/martensite interfaces being favourably orientated for cracking than for a sample pulled in the rolling direction (RD-bar). Also, since DP steels are processed through hot and cold rolling, some anisotropy may be present in terms of metallurgical texture.

Furthermore, although a linear relationship was obtained between $\log(K)$ and $\log(e_f$ (mean)), a significant scatter was observed in the measured e_f values for the DP800 Mini2 specimens (K=3.23). Less scatter was observed in the similar sized DP600 Mini2 specimen (K=2.8). In the Mini2 specimen the necking region is relatively small compared to larger specimens and this smaller region will be more sensitive to less homogeneous microstructures. It is generally accepted that measured failure characteristics of less ductile materials show higher levels of experimental scatter (often quantified via Weibull statistics assuming the weakest link hypothesis). Therefore, for the less homogeneous and less

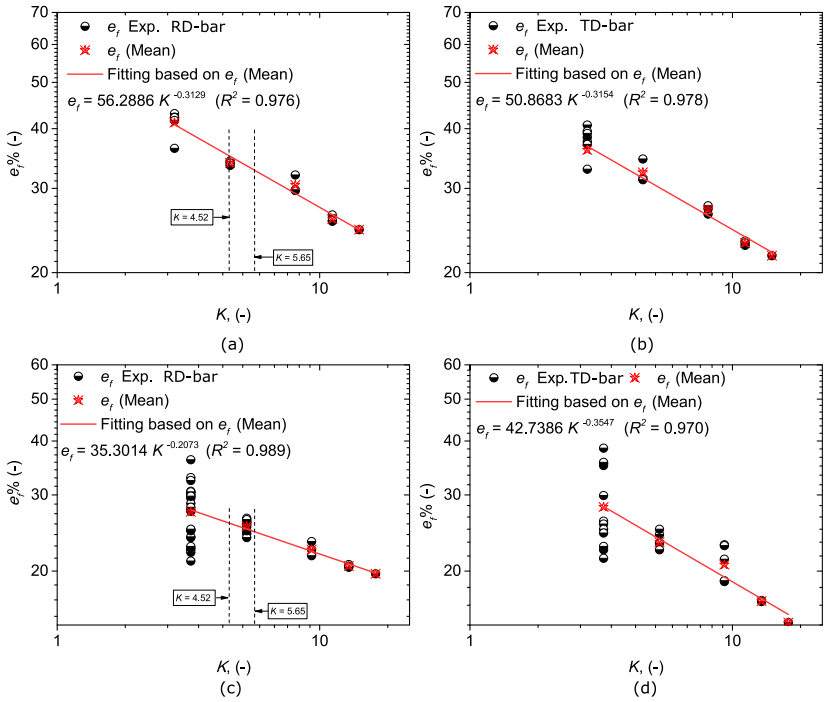

Fig. 3. The relationship between total elongation e_f and tensile specimens' slimness ratio K for DP600 and DP800. (a) DP600 RD-bar, (b) DP600 TD-bar, (c) DP800 RD-bar and (d) DP800 TD-bar. The values of e_0 and α can be determined by the fitting trend-lines' expression.

Table 3
DP600: material constant $\hat{\alpha}$ calculated through method II for both RD-bar and TD-bar. Ref.G and Std. stand for the reference geometry and standard deviation.

Ref.G		$\hat{\alpha}_L^{i\to Ref.G}$	$\hat{\alpha}_L$	Std.	$\hat{\alpha}_T^{i\to Ref.G}$	$\hat{\alpha}_T$	Std.	K range
A80	$\hat{\alpha}^{A50\to A80}$	−0.2192	−0.3011	0.0685	−0.2600	−0.3313	0.0581	(11.18, 14.14)
	$\hat{\alpha}^{ASTM25\to A80}$	−0.3833			−0.3962			(8.07, 14.14)
	$\hat{\alpha}^{Mini1\to A80}$	−0.2833			−0.3546			(4.56, 14.14)
	$\hat{\alpha}^{Mini2\to A80}$	−0.3185			−0.3143			(2.8, 14.14)
A50	$\hat{\alpha}^{A80\to A50}$	−0.2192	−0.3309	0.1187	−0.2600	−0.3643	0.0995	(11.18, 14.14)
	$\hat{\alpha}^{ASTM25\to A50}$	−0.5015			−0.4944			(8.07, 11.18)
	$\hat{\alpha}^{Mini1\to A50}$	−0.3001			−0.3794			(4.56, 11.08)
	$\hat{\alpha}^{Mini2\to A50}$	−0.3353			−0.3235			(2.8, 11.08)
ASTM25	$\hat{\alpha}^{A80\to ASTM25}$	−0.3833	−0.3385	0.1355	−0.3962	−0.3688	0.0986	(8.07, 14.14)
	$\hat{\alpha}^{A50\to ASTM25}$	−0.5015			−0.4944			(8.07, 11.18)
	$\hat{\alpha}^{Mini1\to ASTM25}$	−0.1851			−0.3137			(4.56, 8.07)
	$\hat{\alpha}^{Mini2\to ASTM25}$	−0.2841			−0.2708			(2.8, 8.07)
Mini1	$\hat{\alpha}^{A80\to Mini1}$	−0.2833	−0.2921	0.0880	−0.3546	−0.3171	0.0698	(4.56, 14.14)
	$\hat{\alpha}^{A50\to Mini1}$	−0.3001			−0.3794			(4.56, 11.08)
	$\hat{\alpha}^{ASTM25\to Mini1}$	−0.1851			−0.3137			(4.56, 8.07)
	$\hat{\alpha}^{Mini2\to Mini1}$	−0.4000			−0.2206			(2.8, 4.56)
Mini2	$\hat{\alpha}^{A80\to Mini2}$	−0.3185	−0.3345	0.0486	−0.3143	−0.2823	0.0471	(2.8, 14.14)
	$\hat{\alpha}^{A50\to Mini2}$	−0.3353			−0.3235			(2.8, 11.08)
	$\hat{\alpha}^{ASTM25\to Mini2}$	−0.2841			−0.2708			(2.8, 8.07)
	$\hat{\alpha}^{Mini1\to Mini2}$	−0.4000			−0.2206			(2.8, 4.56)

ductile DP800 material, a greater level of experimental scatter would be expected. Fractographic analysis of the failed tensile specimens was conducted to determine the possible reasons for this phenomenon, as showed in Fig. 4. The results indicate that for DP800 cases with higher e_f values, e.g., Fig. 4(a) and (b), there is little evidence of cracks due to martensite at the fracture surface. Fig. 4(a) and (b) correspond to higher ductilities and a greater final reduction of the specimen cross sectional area. For the cases with lower e_f values, e.g., Fig. 4(e) and (f), cracks associated with martensite can be seen. These cracks appear on a plane, normal to sheet thickness and are consistent with the location of Martensite bands observed in the figure. Failure at Martensite has been observed and these cracks have led to the earlier fracture of these MTS cases. The smaller necking region in Mini2 specimens renders them more prone to experimental scatter in ductility measurements for less homogeneous and less ductile materials. More work may need to be conducted, electron backscatter diffraction (EBSD) and multiscale modelling for instance, to further understand the failure mechanics of the miniatured samples of advanced high strength steel (AHSS), as the work did for duplex stainless steel (DSS) by Dong et al. [21].

3.2. $\hat{e_0}$ and $\hat{\alpha}$ determination through Method II

The specific elongation and the material constant were calculated, based on different geometries, through Method II, which has been introduced in Section 2.3.3. Table 3, Table 4, Tables 5 and 6 showed the material constant and specific elongation values for DP600 and DP800, respectively. By using the calculated specific elongation and material constant values, the trend lines were plotted in Fig. 5.

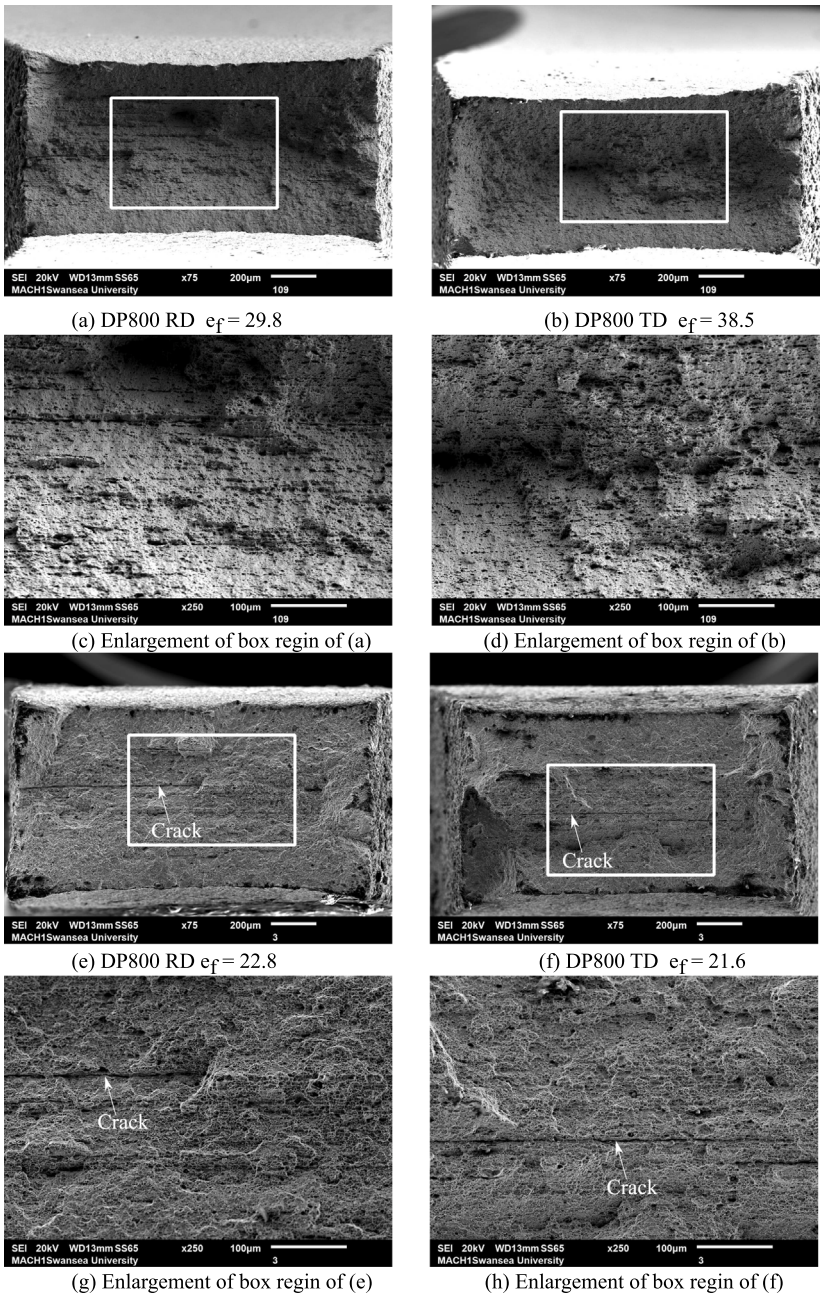

Fig. 4. Scanning Electron Microscope (SEM) images to show the fracture surface of DP800 Mini2 specimens with different e_f values. The cracks were found in the bars with small value of e_f.

3.3. Material constants comparison between Method I and II

Fig. 6 shows the comparison of the specific elongation and material constant obtained from Method I and Method II for DP600 and DP800 steels. For both specific elongation (e_0 v.s. $\hat{e_0}$) and material constant (α v.s. $\hat{\alpha}$), the value differences are observed. The main reason for this difference is due to the methods used to calculate these constants. Method I is to fitting all the e_f data in a larger K range, however, Method II is to use two existed e_f and K to first calculate material constant and then determine the specific elongation. These constants are based on a limited range of K value. The range is decided by the reference geometry and another existed e_f result, which used to calculate constants.

The differences open a question: which set of specific elongation and material constant values can predict e_f more precisely? Figs. 7 and 8 show the comparison of e_f between the predict value and the actual value for DP600 and DP800, respectively. The e_f prediction values (y-axis) were made base on method I and II and the actual e_f values (x-axis) are experimental results. The results show that for DP600, the results indicate that the differences in e_f predicted by Method I is less than 5% across the whole K range. This is true for both RD and TD bars. In terms of the percentage difference in e_f predicted by Method II, by using reference e_f, K and $\hat{\sigma}$, for the standard specimens, $K \in (11.18, 14.14)$, the percentage is less than 4% which is similar to the percentages predicted by using Method I. However, it is also noticed that by using this method to predict e_f, larger percentage differences, although still less than 10%, may arise for the smaller K value specimens. Similar to DP600, for DP800, the predicted e_f values obtained by using Method I give small percentage differences across the whole K range. The T-bar produces larger percentage differences which echoes the previous results.

Table 4
DP600: specific elongation $\hat{e_0}$ calculation through method II for both RD-bar and TD-bar. Ref.G and Std. stand for the reference geometry and standard deviation.

Ref.G		$\hat{e_0}_L^{i\to Ref.G}$	$\hat{e_0}_L$	Std.	$\hat{e_0}_T^{i\to Ref.G}$	$\hat{e_0}_T$	Std.	K range
A80	$\hat{e_0}^{A50\to A80}$	43.9709	55.2928	10.0177	43.2127	52.6511	8.0013	(11.18, 14.14)
	$\hat{e_0}^{ASTM25\to A80}$	67.9066			61.9855			(8.07, 14.14)
	$\hat{e_0}^{Mini1\to A80}$	52.1040			55.5174			(4.56, 14.14)
	$\hat{e_0}^{Mini2\to A80}$	57.1897			49.8886			(2.8, 14.14)
A50	$\hat{e_0}^{A80\to A50}$	43.9709	60.6320	18.4954	43.2127	58.8256	14.1251	(11.18, 14.14)
	$\hat{e_0}^{ASTM25\to A50}$	86.9200			76.0823			(8.07, 11.18)
	$\hat{e_0}^{Mini1\to A50}$	53.4476			57.6439			(4.56, 11.08)
	$\hat{e_0}^{Mini2\to A50}$	58.1895			50.3634			(2.8, 11.08)
ASTM25	$\hat{e_0}^{A80\to ASTM25}$	68.2371	63.5685	23.3643	70.6651	67.4204	18.5705	(8.07, 14.14)
	$\hat{e_0}^{A50\to ASTM25}$	93.9841			92.1758			(8.07, 11.18)
	$\hat{e_0}^{Mini1\to ASTM25}$	39.8901			56.5203			(4.56, 8.07)
	$\hat{e_0}^{Mini2\to ASTM25}$	52.1626			50.3203			(2.8, 8.07)
Mini1	$\hat{e_0}^{A80\to Mini1}$	52.4257	54.3304	11.0123	61.7803	57.1992	8.7373	(4.56, 14.14)
	$\hat{e_0}^{A50\to Mini1}$	54.4909			65.4069			(4.56, 11.08)
	$\hat{e_0}^{ASTM25\to Mini1}$	41.8114			56.2309			(4.56, 8.07)
	$\hat{e_0}^{Mini2\to Mini1}$	68.5934			45.3785			(2.8, 4.56)
Mini2	$\hat{e_0}^{A80\to Mini2}$	56.1653	57.7658	4.5958	55.7863	53.1017	3.9565	(2.8, 14.14)
	$\hat{e_0}^{A50\to Mini2}$	57.7078			56.6185			(2.8, 11.08)
	$\hat{e_0}^{ASTM25\to Mini2}$	53.1442			52.0205			(2.8, 8.07)
	$\hat{e_0}^{Mini1\to Mini2}$	64.0458			47.9814			(2.8, 4.56)

Table 5
DP800: material constant $\hat{\alpha}$ calculated through method II for both RD-bar and TD-bar. Ref.G and Std. stand for the reference geometry and standard deviation.

Ref.G		$\hat{\alpha}_L^{i\to Ref.G}$	$\hat{\alpha}_L$	Std.	$\hat{\alpha}_T^{i\to Ref.G}$	$\hat{\alpha}_T$	Std.	K range
A80	$\hat{\alpha}^{A50\to A80}$	−0.1763	−0.2090	0.0247	−0.4846	−0.4478	0.0838	(12.91, 16.33)
	$\hat{\alpha}^{ASTM25\to A80}$	−0.2309			−0.5489			(9.32, 16.33)
	$\hat{\alpha}^{Mini1\to A80}$	−0.2250			−0.3777			(5.27, 16.33)
	$\hat{\alpha}^{Mini2\to A80}$	−0.2037			−0.3800			(3.23, 16.33)
50	$\hat{\alpha}^{A80\to A50}$	−0.1763	−0.4478	0.0402	−0.4846	−0.4480	0.1155	(12.91, 16.33)
	$\hat{\alpha}^{ASTM25\to A50}$	−0.2702			−0.5953			(9.32, 12.91)
	$\hat{\alpha}^{Mini1\to A50}$	−0.2378			−0.3497			(5.27, 12.91)
	$\hat{\alpha}^{Mini2\to A50}$	−0.2083			−0.3623			(3.23, 12.91)
ASTM25	$\hat{\alpha}^{A80\to ASTM25}$	−0.2309	−0.2274	0.0335	−0.3962	−0.4110	0.1899	(9.32, 16.33)
	$\hat{\alpha}^{A50\to ASTM25}$	−0.2702			−0.5953			(9.32, 12.91)
	$\hat{\alpha}^{Mini1\to ASTM25}$	−0.2193			−0.2091			(5.27, 9.32)
	$\hat{\alpha}^{Mini2\to ASTM25}$	−0.1893			−0.2906			(3.23, 9.32)
Mini1	$\hat{\alpha}^{A80\to Mini1}$	−0.2250	−0.2091	0.0373	−0.3777	−0.3305	0.0823	(5.27, 16.33)
	$\hat{\alpha}^{A50\to Mini1}$	−0.2378			−0.3497			(5.27, 12.91)
	$\hat{\alpha}^{ASTM25\to Mini1}$	−0.2193			−0.2091			(5.27, 9.32)
	$\hat{\alpha}^{Mini2\to Mini1}$	−0.1544			−0.3853			(3.23, 5.27)
Mini2	$\hat{\alpha}^{A80\to Mini2}$	−0.2037	−0.1889	0.0244	−0.3800	−0.3546	0.0438	(3.23, 16.33)
	$\hat{\alpha}^{A50\to Mini2}$	−0.2083			−0.3623			(3.23, 12.91)
	$\hat{\alpha}^{ASTM25\to Mini2}$	−0.1893			−0.2906			(3.23, 9.32)
	$\hat{\alpha}^{Mini1\to Mini2}$	−0.1544			−0.3853			(3.23, 5.27)

3.4. Miniaturized tensile specimens' performance

3.4.1. Performance on predicting e_f

Non-standard miniaturized tensile specimens, Mini1 and Mini2, were original designed for the RAP process. It is important to know if the e_f values obtained from non-standard MTS and standard test-pieces are comparable. Table 7 shows the e_f value comparison between experimental result (e_f^{exp}, obtained from standard tensile specimens) and predicted e_f results based on Mini1 (e_f^{pre-1}) and Mini2 (e_f^{pre-2}). Error^1 % and Error^2 % stand for the e_f differences in percentage. The results indicated that most of the errors are under 10% as shown in the table. Along with the previous work [7], a comparison of yield strength, tensile strength and the uniform elongation between MTS and the standard tensile specimens, shows that these mechanical properties, obtained using the miniaturized tensile specimen designs in this paper, adequately represent bulk material properties. This gives more confidence in the further use of MTS as part of the RAP process for steel strip products. For the non-standard dimension Mini2 designed for RAP, attention should be paid in terms of prediction to the total elongation value e_f due to this large divergence range.

3.4.2. Performance on predicting FLC of DP800

This section and the following section both focus on predicting the formability of DP800 from small scale samples, produced using the RAP process. DP800 is a high strength steel, yet accurately characterizing its formability is important for designing automotive components where strength is important. Furthermore, here DP800 is used as a test material to see is the process can be used to predict the formability of materials from small scale samples. If successful, this provides confidence in using the method to evaluate the formability of new alloys, developed using the RAP method. Fig. 9 showed the values of strain hardening exponent (n) and strength coefficient (k) based on A80 and Mini1. The results showed that the n value predicted through Mini1 bar is larger than that predicted by A80 bar. The over predicted n value means DP800 is 'more ductile' through Mini1's prediction. Compared to the previous research [22], the dashed line in Fig. 9(a), Mini1's n value is still higher. This is mainly due to the designed non-standard miniaturized Mini1 predicted a relative lower value of ultimate tensile strength (~10%) [7] and also may due to the mini bars may experience greater deformation before necking occurs due to the geometry of the specimen. However, the reported strength coefficients are similar, as showed in Fig. 9(b).

Table 6
DP800: specific elongation $\hat{\varepsilon}_0$ calculation through method II for both RD-bar and TD-bar. Ref.G and Std. stand for the reference geometry and standard deviation.

Ref.G		$\hat{\varepsilon}_{0L}^{i\to Ref.G}$	$\hat{\varepsilon}_{0L}$	Std.	$\hat{\varepsilon}_{0T}^{i\to Ref.G}$	$\hat{\varepsilon}_{0T}$	Std.	K range
A80	$\hat{\varepsilon}_0^{A50\to A80}$	32.2341	35.3765	2.4032	58.8341	54.2091	12.9239	(11.18, 14.14)
	$\hat{\varepsilon}_0^{ASTM25\to A80}$	37.5415			70.4161			(8.07, 14.14)
	$\hat{\varepsilon}_0^{Mini1\to A80}$	36.9344			43.6529			(4.56, 14.14)
	$\hat{\varepsilon}_0^{Mini2\to A80}$	34.7960			43.9334			(2.8, 14.14)
A50	$\hat{\varepsilon}_0^{A80\to A50}$	32.2341	36.4831	3.7466	58.8341	55.4055	17.0131	(11.18, 14.14)
	$\hat{\varepsilon}_0^{ASTM25\to A50}$	40.9849			84.6674			(8.07, 11.18)
	$\hat{\varepsilon}_0^{Mini1\to A50}$	37.7275			41.6658			(4.56, 11.08)
	$\hat{\varepsilon}_0^{Mini2\to A50}$	34.9858			43.0304			(2.8, 11.08)
ASTM25	$\hat{\varepsilon}_0^{A80\to ASTM25}$	37.5415	37.3309	2.8089	76.3455	59.9172	24.1920	(8.07, 14.14)
	$\hat{\varepsilon}_0^{A50\to ASTM25}$	40.9849			92.1758			(8.07, 11.18)
	$\hat{\varepsilon}_0^{Mini1\to ASTM25}$	36.5830			35.7604			(4.56, 8.07)
	$\hat{\varepsilon}_0^{Mini2\to ASTM25}$	34.2141			42.8954			(2.8, 8.07)
Mini1	$\hat{\varepsilon}_0^{A80\to Mini1}$	36.9344	36.0225	2.1716	47.6043	44.3046	5.6832	(4.56, 14.14)
	$\hat{\varepsilon}_0^{A50\to Mini1}$	37.7275			45.4374			(4.56, 11.08)
	$\hat{\varepsilon}_0^{ASTM25\to Mini1}$	36.5830			35.9686			(4.56, 8.07)
	$\hat{\varepsilon}_0^{Mini2\to Mini1}$	32.8452			48.2080			(2.8, 4.56)
Mini2	$\hat{\varepsilon}_0^{A80\to Mini2}$	34.7960	34.2103	0.9674	42.7818	41.5646	2.0835	(2.8, 14.14)
	$\hat{\varepsilon}_0^{A50\to Mini2}$	34.9858			41.9024			(2.8, 11.08)
	$\hat{\varepsilon}_0^{ASTM25\to Mini2}$	34.2141			38.5268			(2.8, 8.07)
	$\hat{\varepsilon}_0^{Mini1\to Mini2}$	32.8452			43.0477			(2.8, 4.56)

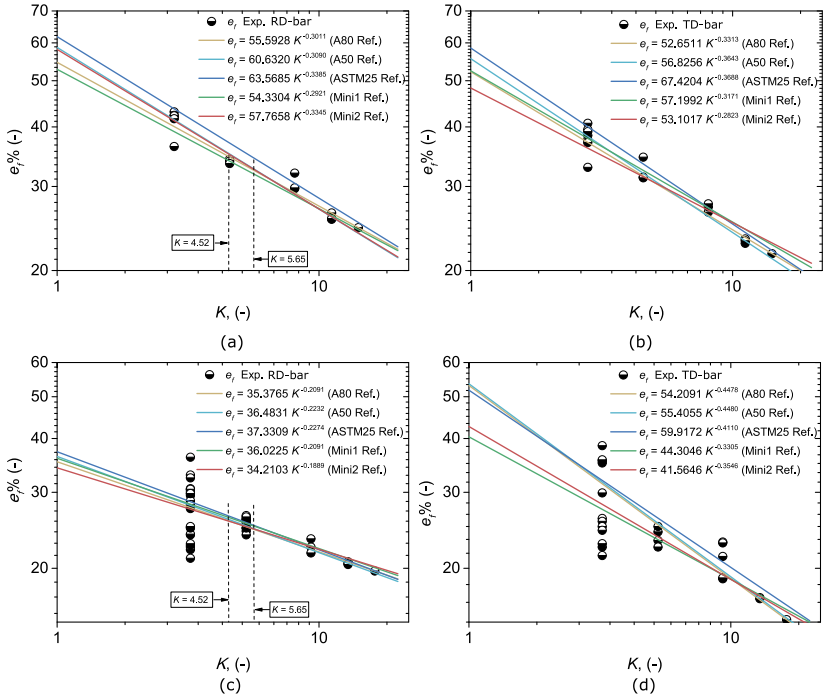

Fig. 5. The relationship between total elongation e_f and the tensile specimens' slimness ratio K for DP600 and DP800. (a) DP600 RD-bar, (b) DP600 TD-bar, (c) DP800 RD-bar and (d) DP800 TD-bar. The modified material constants can be determined based on different reference geometries.

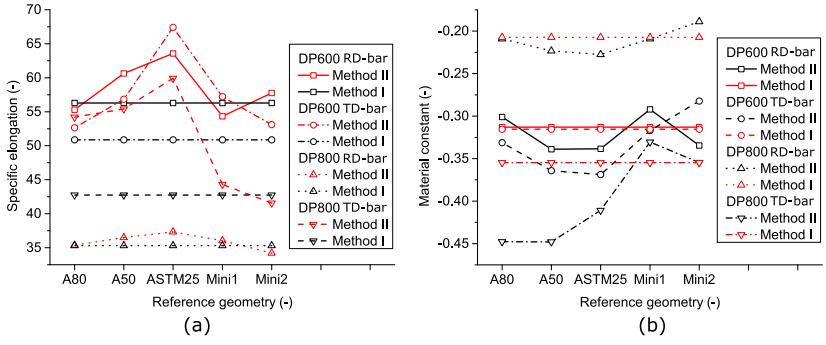

Fig. 6. The comparison of specific elongation (a) and material constant (b) obtained from Method I and II for DP600 and DP800 steel.

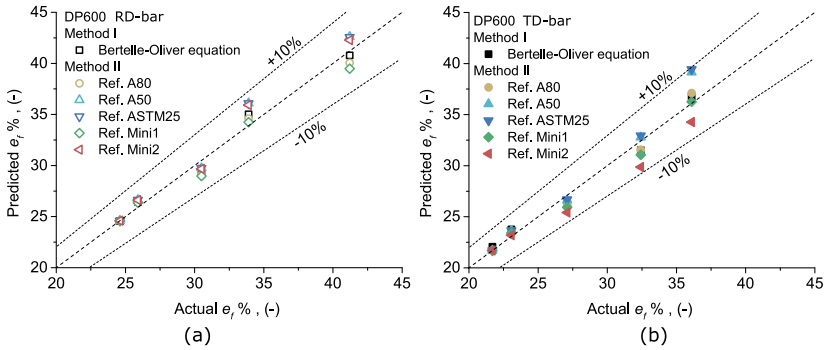

Fig. 7. The comparison of material constant obtained from method I and II for DP600. (a) RD-bar and (b) TD-bar.

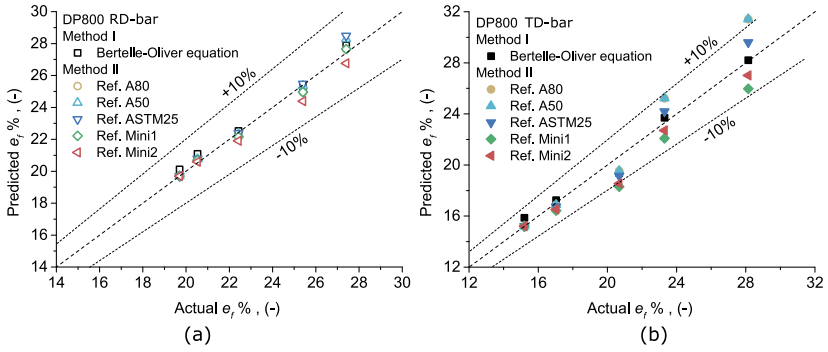

Fig. 8. The comparison of material constant obtained from method I and II for DP800. (a) RD-bar and (b) TD-bar.

Table 7
The comparison of total elongation between the experiment results (e_f^{exp}) and the predicted results based on Mini1 (e_f^{pre-1}) and Mini2 (e_f^{pre-2}) for both RD-bars and TD-bars. Error[1] % and Error[2] % stand for the e_f differences in percentage.

Steel	Dimension	RD-bars					TD-bars				
		e_f^{exp} (Mean)	e_f^{pre-1}	Error[1] %	e_f^{pre-2}	Error[2] %	e_f^{exp} (Mean)	e_f^{pre-1}	Error[1] %	e_f^{pre-2}	Error[2] %
DP600	A80	24.60	21.56	12.37	21.56	12.37	21.70	25.25	16.38	25.26	16.39
	A50	25.90	23.68	8.57	23.68	8.57	23.07	26.6	15.3	26.6	15.3
	ASTM25	30.50	26.98	11.55	26.98	11.55	27.10	28.58	5.46	28.58	5.46
DP800	A80	19.70	21.34	8.31	21.34	8.33	15.20	15.07	0.86	15.81	0.81
	A50	20.53	22.13	7.76	22.13	7.77	17.03	16.5	3.14	16.51	3.1
	ASTM25	22.43	23.27	3.76	23.27	3.78	20.68	18.77	9.55	18.72	9.51

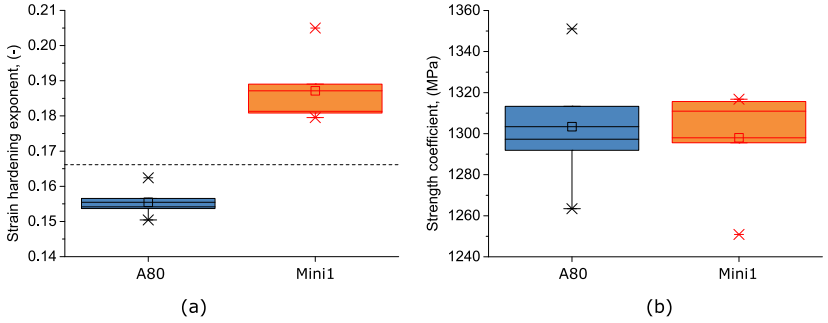

Fig. 9. The comparison of strain hardening exponent and strength coefficient based on A80 and Mini1. (a) strain hardening exponent and (b) strength coefficient. The predicted n value through Mini1 is higher than that predicted by A80, however, the predicted strength coefficients are similar. The dashed line denotes the reported n value in the work of [22].

Fig. 10 shows the forming limit curves of DP800 based on strain hardening exponents of A80 and Mini1. The results showed that the FLC based on Mini1's prediction is upper to that predicted by standard A80 dimension and other previous research. This is due to the larger n value for Mini1's prediction, which makes DP800 a 'more ductile' steel compare to what it should be. Therefore, attention should be given whilst the miniaturized non-standard Mini1's results used to predict the formability of DP800 strip obtained from the RAP routine.

3.4.3. Performance on predicting r-value of DP800

Fig. 11 showed the relationship between r-value and the tensile bars' orientation. Four tensile bars' dimensions, both standard bars (A80,

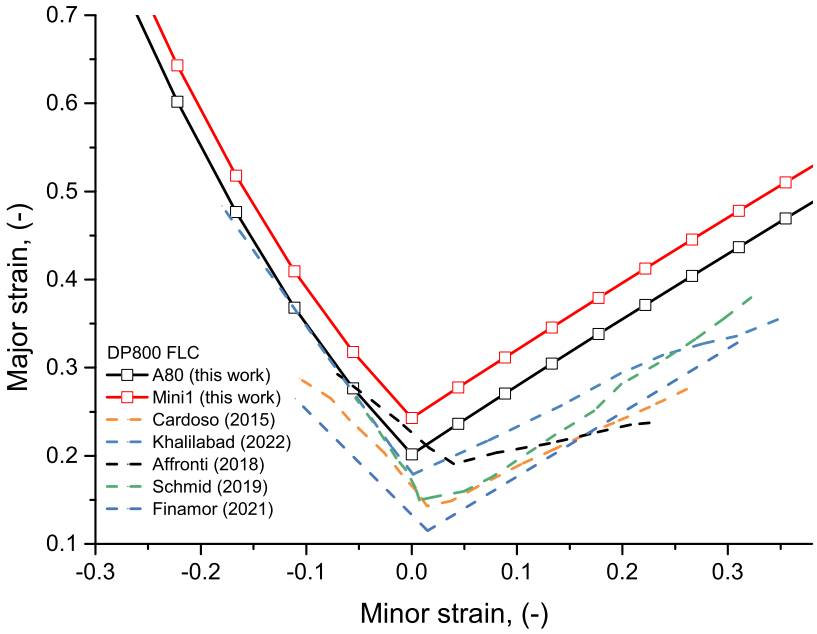

Fig. 10. Forming limit curves (FLC) of DP800 this work (solid lines) and previous research (dashed lines). Tensile tests results (black and red circles), based on A80 and Mini1 bars were also added. The predicted FLC by using Mini1 (in red) is upward offset to the FLC predicted by A80 (in black) and FLCs in the previous work. Cardoso (2015), Khallabad (2022), Affronti (2018), Schimid (2019) and Finamor (2021) denote the references of [22–26], respectively, in this work.

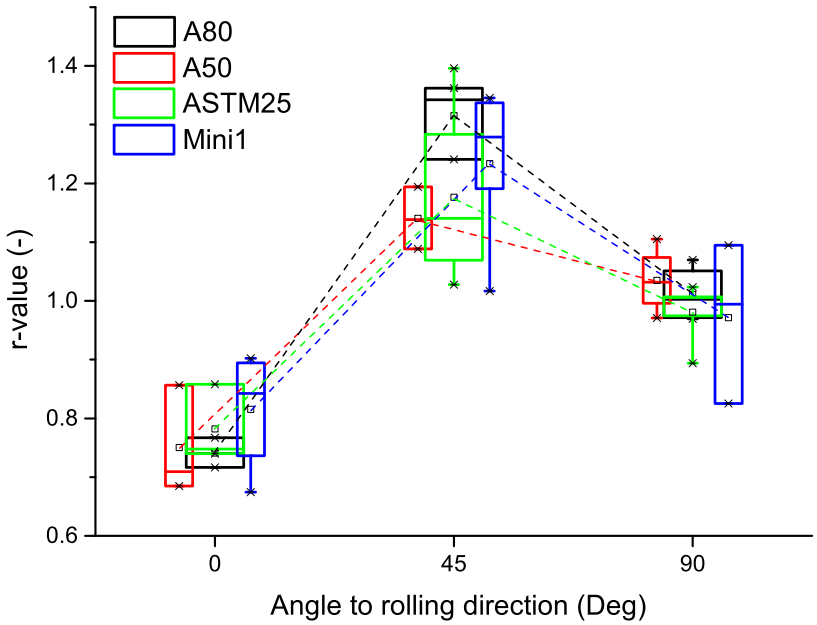

Fig. 11. Experimental results of DP800 r-value based on A80, A50, ASTM25 and Mini1 tensile specimens. All r-value results obtained from different size of specimens give same trends: $r_{45°} > r_{90°} > r_{0°}$, even for the non-standard miniaturized specimen Mini1.

A50 and ASTM25) and non-standard miniaturized bar (Mini1), were selected and therefore four groups of data were obtained, as showed in figure. There data obtained from standard dimension tensile bar show a similar r-value trend: $r_{45°} > r_{90°} > r_{0°}$. This trend was similar to the previous limited research, which has been discussed in details in the work of Zhang et al. [27]. For the results obtained by Mini1, it echoes the trend predicted by the standard bars, although some scatters are observed. This scatter is also observed in the predictions by the standard bars. In terms of the magnitudes of r-value, the results predicted by Mini1 are in a similar range compared to those predicted by the standard bars. This is true for all the orientation. It is worth mentioning that the Mini1 design is valid to predict Interstitial Free (IF) steel's r-value [28]. This will give more confidence to use Mini1 design for the RAP routine strip to predict synthetic DP800 r-value as well as evaluating anisotropy in similar materials produced through the RAP process.

4. Conclusions

The work presented in this paper investigates the ability of characterizing the mechanical properties of DP steels using miniaturized tensile specimen of a sized suitably for manufacture using small scale RAP samples. Specifically, the ductility, forming limit and r-values have been evaluated against those measured from full sized standard tensile specimens. The conclusions of the work are:

1. The Bertelle–Oliver equation can be used to accurately correlate the total elongation, e_f, to test-piece's slimness ratio, K, for all specimen sizes studied for both DP600 and DP600. This is despite the sheet thicknesses being less than the critical value of 4 mm specified by the standard. Furthermore, the tensile strength of DP800 exceeds the maximum value of 700 MPa, specified for the Bertelle–Oliver method. This provides confidence in using this method to predict total elongation for other similar materials, developed using RAP. However, some caution must be used when using the smallest tensile specimen, Mini2, as there is significant scatter in the e_f values obtained. For this and similar alloys, the slightly larger Mini1 sample would be more suitable.
2. The coefficients for the Bertelle–Oliver equation were evaluated for both DP600 and DP800 tensile specimens tested both along and transverse to the rolling direction. For DP600 the constants e0 and alpha varied little between those obtained in each direction. However, test-piece orientation had a more significant effect on the values of these constants for DP800, indicating that orientation has more influence on the total elongation behaviour in the higher strength, lower ductility steel.
3. For DP800, the strain hardening exponents, n, were obtained from tensile curves calculated from the A800 and Mini1 specimen. These values were used to estimate forming limit curves using the Keeler–Brazier method. Due to a higher strain hardening exponent, the FLC estimated from the Mini1 tensile data exhibits a higher value of major strain than that estimated from the A80 data. However, when comparing to previous studies, both methods over predict major strain however, the trend is similar. Furthermore, when plotting data points for tensile tests on the FLC plot, these occur at lower values of major strain.
4. The anisotropy of DP800 has been characterized using both standard tensile specimens and Mini1. Some scatter is observed, but the trend in r-values obtained at 0°, 45° and 90° to the rolling direction is similar.

The overall objective of this research was to be able to gain confidence in the ability to predict the forming behaviour of heterogeneous alloys such as dual phase steels, from total elongation, e_f, from small scale tensile tests, such as those manufactured from RAP samples. The results show that despite the miniature specimens exceeding the limits specified for the Bertelle–Oliver rule, total elongation from these specimens can be used to extrapolate values that would be obtained from standard tensile bars, allowing an assessment of ductility of 40 g of materials produced by RAP. Furthermore, estimates of forming limit curves and anisotropy can be made using this method, with levels of confidence similar to those obtained from full-sized standard tensile specimens.

CRediT authorship contribution statement

Lintao Zhang: Conceptualization, Methodology, Software, Data curation, Writing – original draft, Visualization, Investigation. **Will Harrison:** Conceptualization, Methodology, Software, Data curation, Writing – original draft. **Mazher A. Yar:** Visualization, Investigation. **Shahin Mehraban:** Data curation, Writing – original draft, Visualization, Investigation. **Stephen G.R. Brown:** Writing – review & editing, Supervision, Funding. **Nicholas P. Lavery:** Writing – review & editing, Supervision, Funding.

Declaration of competing interest

The authors declare that they have no known competing financial interests or personal relationships that could have appeared to influence the work reported in this paper.

Data availability

No data was used for the research described in the article.

Acknowledgements

The authors would like to thank EPSRC, UK for funding the Rapid Alloy Prototyping Prosperity Partnership project (EP/S005218/1 - ACCELERATING ALLOY DEVELOPMENT THROUGH DELIVERING NOVEL PROTOTYPING SOLUTIONS) which made this work possible. The authors would also like to thank the Welsh Government, European Regional Development Fund (ERDF) and SMART Expertise Wales for funding Materials Advanced Characterization Centre (MACH1) where the work was carried out.

References

[1] Y. Granbom, Structure and Mechanical Properties of Dual Phase Steels – an Experimental and Theoretical Analysis (PhD dissertation), Royal Institute of Technology, 2010.
[2] X. Yu, Optimisation of the Microstructure and Mechanical Properties of DP800 Strip Steel, (Master's Thesis), Swansea University, Swansea, UK, 2005.
[3] C. Lesch, N. Kwiaton, F.N. Klose, Advanced high strength steels (AHSS) for automotive applications tailored properties by smart microstructural adjustment, Steel Res. Int. 88 (10) (2017) 1700210.
[4] D. Farrugia, S. Brown, N.P. Lavery, P. Cameron, C. Davis, Rapid alloy prototyping for a range of strip related advanced steel grades, Proc. Manuf. 50 (2020) 784–790.
[5] Y. Zhu, C. Slater, S. Connolly, D. Farrugia, C. Davis, Rapid alloy prototyping for strip steel development: DP800 steel case study, Ironmak. Steelmak. 48 (5) (2021) 493–504.
[6] J.H. Wen, L.J. Zhang, J. Ning, F. Xue, X.W. Lei, J.X. Zhang, S.J. Na, Laser additively manufactured intensive dual-phase steels and their microstructures, properties and corrosion resistance, Mater. Des. 192 (2020) 108710.
[7] L. Zhang, W. Harrison, M.A. Yar, S.R.G. Brown, N.P. Lavery, The development of miniature tensile specimens with non-standard aspect and slimness ratios for rapid alloy prototyping processes, J. Mater. Res. Technol. 15 (2021) 1830–1843.
[8] J.R. Davis, Tensile Testing, second ed., 2004.
[9] W. Yang, L. Wang, Z. Song, X. Luo, G. Zhang, Tensile plasticity of miniature specimens for a low alloy steel investigated by digital image correlation technique, Steel Res. Int. 92 (2021) 2000685.
[10] X. Xu, X. Zhao, Y. Ai, M. Liang, N. Li, W. Lin, C. Qin, Study and analysis on the tensile test elongation variation law for high-strength pipeline steel, J. Mater. Eng. Perform. 29 (2020) 2164–2171.
[11] Y. Takeda, C. Kiattisaksri, M. Aramaki, S. Munetoh, O. Furukimi, Effects of specimen thickness in tensile tests on elongation and deformation energy for industrially pure iron, ISIJ Int. 57 (6) (2017) 1129–1137.
[12] D.N. Hanlon, D.M.C. Bohemen, S. Celotto, Critical assessment 10: tensile elongation of strong automotive steels as function of testpiece geometry, Mater. Sci. Technol. 31 (4) (2015) 385–388.
[13] G.M. Cola, J.B. Hanhold, T. Lolla, B. Radhakrishnan, S. Babu, On the total elongation of advanced high-strength steels, Iron Steel Technol. 10 (2013) 1–7.
[14] International Organization for Standardization, Steel-Conversion of Elongation Values-Part 1: Carbon and Low Alloy Steels, ISO 2566-1, 1984.
[15] BSI British Standards, Metallic materials — tensile testing Part 1: method of test at ambient temperature, 2009.
[16] D.A. Oliver, Proposed new criteria of ductility from a new law connecting the percentage elongation with size of test-piece, Proc. Inst. Mech. Eng. 115 (1) (1928) 827–864.
[17] S.P. Keeler, W.G. W.G. Brazier, Relationship between laboratory material characterization and press-shop formability, Proc. Conf. Microalloy 75 (1977) 517–528.
[18] J.H. Hollomon, Tensile deformation, Trans. Metall. Soc. AIME 162 (1945) 268–290.
[19] ASTM E8/E8M-13a Standard test methods for tension testing of metallic materials, 2013.
[20] ISO 6892–1 Metallic materials–tensile testing–Part 1: method of test at room temperature, 2019.
[21] Z. Dong, X.F. Xie, W. Jiang, W. Wan, X. Zhai, X. Zhao, Microstructure-based multiscale and heterogeneous elasto-plastic properties of 2205 duplex stainless steel welded joints: Experimental and modeling, Int. J. Plast. 159 (2022) 103474.
[22] M.C. Cardoso, L.P. Moreira, Forming limit analysis of DP600-800 steels, Int. J. Mater. Metall. Eng. 9 (9) (2015) 1123–1130.
[23] M.M. Khalilabad, E.S. Perdahcıoglu, E.H. Atzema, A.H. Boogaard, An in-plane bending test to characterize edge ductility in high-strength steels, J. Mater. Eng. Perform. (2022) 1–13.
[24] E. Affronti, M. Weidinger, M. Merklein, Metallographic analysis of failure mechanisms during Nakajima tests for the evaluation of forming limits on a dual phase steel, IOP Conf. Ser. Mater. Sci. Eng. 418 (2018) 012047.

[25] H. Schmida, P. Hetza, M. Merklein, Failure behavior of different sheet metals after passing a drawbead, in: 47th SME North American Manufacturing Research Conference, Penn State Behrend Erie, Pennsylvania, 2019.

[26] F.P. Finamor, M.A. Wolff, V.S. Lage, Prediction of forming limit diagrams from tensile tests of automotive grade steels by a machine learning approach, IOP Conf. Ser. Mater. Sci. Eng. 1157 (2021) 012080.

[27] L. Zhang, W. Harrison, S. Mehraban, S.G.R. Brown, N.P. Lavery, Size effect on the post-necking behaviour of Dual-phase 800 Steel: modelling and experiment, Materials 16 (4) (2023) 1458.

[28] T.S. Abdullah, L. Zhang, P. Evans, G. Lodwig, N.P. Lavery, Scaling effects in miniaturised tensile testing on mechanical properties and plastic anisotropy r-values in Interstitial Free Steel, J. Mater. Res. Technol (2023) (submitted for publication).